Simulated Changes in the Frequency of Extremes and Regional Features of Seasonal/Annual Temperature and Precipitation when Atmospheric CO_2 Is Doubled

T. YONETANI

National Research Institute for Earth Science and Disaster Prevention, Tsukuba, Japan

HAL B. GORDON

Division of Atmospheric Research, CSIRO, Aspendale, Victoria, Australia

(Manuscript received 9 September 1999, in final form 11 August 2000)

ABSTRACT

Following a transient increase in the atmospheric carbon dioxide to double the current level, and a subsequent maintenance at the doubled level, there is a climate shift toward a new equilibrium state. Changes in the mean temperature and precipitation, and changes in the occurrence frequencies of their extremes for the doubled carbon dioxide conditions have been assessed at the continental scale. There is a characteristic spatial pattern that involves a maximum annual mean warming in high northern latitudes and a minimum annual mean warming around Antarctica and in the northern North Atlantic. Under maintained doubled carbon dioxide, this interhemispheric asymmetry disappears except for an ocean–land asymmetry. A possible mechanism for this is considered in terms of changes in effective thermal capacity due to a reduction of overturning in the oceans that continues to decline after the atmospheric carbon dioxide stops increasing. It is also found that global warming becomes most noticeable in the occurrence frequency of high extremes in the annual mean temperature in the low latitudes, even though the temperature rise is largest in the high northern latitudes in autumn and winter. In addition, extremes of large (small) annual and seasonal total precipitation are recorded much more frequently in regions where the mean precipitation increases (decreases).

1. Introduction

Many numerical experiments have been conducted to obtain an estimate of the climatic effects of future changes in the atmospheric composition due to human activities. Because large impacts on the environment and human society will arise from changes in the frequency of occurrence of climatic extremes, possible future changes in various aspects of weather and climate extremes have been studied in more detail in recent years using global climate models with improved resolution, high-resolution regional models, and statistical downscaling techniques (Meehl et al. 2000). For example, there have been a number of papers examining the changes in simulated extreme daily values such as minimum and maximum surface temperature and daily precipitation (Rind et al. 1989; Cao et al. 1992; Gordon et al. 1992; Whetton et al. 1993; Gregory and Mitchell 1995; Hennessy and Pittock 1995; Mearns et al. 1995; Hennessy et al. 1997; Mason and Joubert 1997; Giorgi et al. 1998; Zwiers and Kharin 1998; McGuffie et al. 1999; Solman and Nuñez 1999; Colombo et al. 1999). Changes in tropical cyclone numbers and intensity in a warmer climate have been investigated (Bengtsson et al. 1996; Knutson et al. 1998; Krishnamurti et al. 1998; Knutson and Tuleya 1999; Druyan et al. 1999) and also extratropical storms (Katzfey and McInnes 1996; Beersma et al. 1997; Carnell and Senior 1998; Lunkeit et al. 1998; Schubert et al. 1998; Ulbrich and Christoph 1999). The relation between changes in the frequency of extremes, shifts in the means and changes in the variability has also been examined in a theoretical way (Mearns et al. 1984; Wigley 1985; Katz and Brown 1992). In addition to changes of extremes, attention has been drawn to spatial patterns of changes such as El Niño-like responses and an interhemispheric asymmetry of warming (Kattenberg et al. 1996). A number of climate change experiments indicated that increasing greenhouse gases may cause an El Niño–like change (Knutson and Manabe 1995, 1998; Meehl and Washington 1996; Timmermann et al. 1999), although some diverse results have been obtained (Tett 1995; Cane et al. 1997).

The purpose of this paper is to illustrate the changes in the occurrence frequency of extremes of seasonal

Corresponding author address: Dr. T. Yonetani, National Research Institute for Earth Science and Disaster Prevention, Tsukuba, Ibaraki 305-0006, Japan.
E-mail: yonetz@bosai.go.jp

mean surface air temperature and seasonal total precipitation, and the evolution of the spatial features of the changes, due to global warming by comparing the climate model simulation with $1 \times CO_2$ to future simulated climate states with $2 \times CO_2$. We have conducted two multicentury climate model runs to clarify changes in extremes under sustained $2 \times CO_2$ conditions. The first consists of a climate change experiment with CO_2 increased to $2 \times CO_2$, and then held constant for more than 800 yr. The second is a companion control run ($1 \times CO_2$) of the same length. Seasonal and annual values of temperature and precipitation obtained from these very long runs will be used to project possible changes in climate at the global and regional scales.

Regional climate is subject to time variations from low frequencies to high frequencies and some regional climate changes have been shown to be teleconnected phenomena (Nicholls et al. 1996). In addition to low-frequency changes that occur in the present climate, a common feature of increasing CO_2 in coupled models and then holding the CO_2 constant at a given level is that the climate keeps on warming (Manabe and Stouffer 1993, 1994). It has also been shown that thermohaline circulation whose intensity is considered to have a considerable effect on magnitude of warming at regional scales (IPCC 1992; Kattenberg et al. 1996) continues changing for some centuries after CO_2 stops increasing (Manabe and Stouffer 1993; Schmittner and Stocker 1999). Thus we have conducted two multicentury climate model runs to clarify changes in extremes and interhemispheric asymmetry of warming under sustained $2 \times CO_2$ conditions.

Extremes of short-term values such as the annual maximum of daily maximum temperature and that of daily precipitation, the annual minimum of daily minimum temperature, maximum wind gusts, etc., have large variations in space and time. For example, a daily precipitation amount that is deemed extraordinarily large judging from a given extreme value distribution may occur at some location prone to heavy rainfall events. This presents a real problem when designing buildings or preventative structures that can cope with occasional extreme events. Such ''outlier'' events makes statistical analysis difficult in many fields because the magnitude is so large or so small that the value might not be considered to come from the same population. On the other hand, changes in the frequency of occurrence of such outliers could be a good indicator of climate change. However, the seasonal means and seasonal totals might not become appreciably larger or smaller despite more or less extreme events with short lifetimes.

In a modeling study of changes in extreme values, it would be desirable to use a fine mesh model that can simulate severe events such as rainstorms, föhn winds in Europe, and other highly localized phenomena. However, the computational burden of carrying out multicentury climate change runs using such a model is prohibitive, and thus we are confined to making estimates using coarse-resolution models as used in this study. In addition, changes in extremes of seasonal and annual temperature and precipitation can have a great socioeconomic impact. In this paper, values that are larger (smaller) than the maximum (minimum) in a 100-yr time series in the $1 \times CO_2$ run will be taken to represent extremes. We investigate how often the seasonal values exceed their extremes during the course of the climate system shifting toward its new equilibrium state under the $2 \times CO_2$ scenario. In an analysis of data such as annual maximum and annual minimum of daily values, it would certainly be inappropriate to use the highest/lowest value out of 100 because of the outlier problem. But the extreme value may not be very far from other record values of seasonal mean temperature and seasonal total precipitation at a grid box representing several hundreds of kilometers square. To ascertain the validity of this assumption and the theoretical soundness of the results, the effects of changes of climatic means and year-to-year variability on the occurrence frequency of the extremes are theoretically considered before analyzing the model data.

There are a number of distribution functions used for frequency analysis and studying variability of meteorological elements. A modified Gumbel distribution has been proposed for wind gusts (Revfeim and Hessell 1984). A three-parameter gamma distribution has been shown to give a good fit to daily temperature and monthly grid box temperatures (Jones et al. 1999). The gamma probability distribution (Gregory and Mitchell 1995; Groisman et al. 1999) and generalized extreme value distribution (Mason and Joubert 1997; Zwiers and Kharin 1998) have been used to study possible changes of extreme daily values due to climate change. A normal distribution has been adopted in climate change impact studies for temperature (Mearns et al. 1984; Hennessy and Pittock 1995). Here we first examine changes in the occurrence frequency of extremes under the assumption that frequency of seasonal mean temperature and seasonal total precipitation at a grid box can be approximated by a normal distribution. The effects of this assumption on the results obtained are considered in the summary and discussion section.

The methodology is described in section 2. The effects of changes in the mean and variance on the occurrence frequency of extremes are considered to have an occurrence probability that is normal. This and the applicability of a Gaussian distribution to the model climate distributions of seasonal/annual values are described in section 3. The data obtained from the long model runs has been assessed for changes in climate at the regional scale and the occurrence frequencies of record-breaking values due to global warming. Results of this analysis are contained in sections 4 and 5 for surface air temperature and precipitation, respectively. There then follows a summary and discussion section.

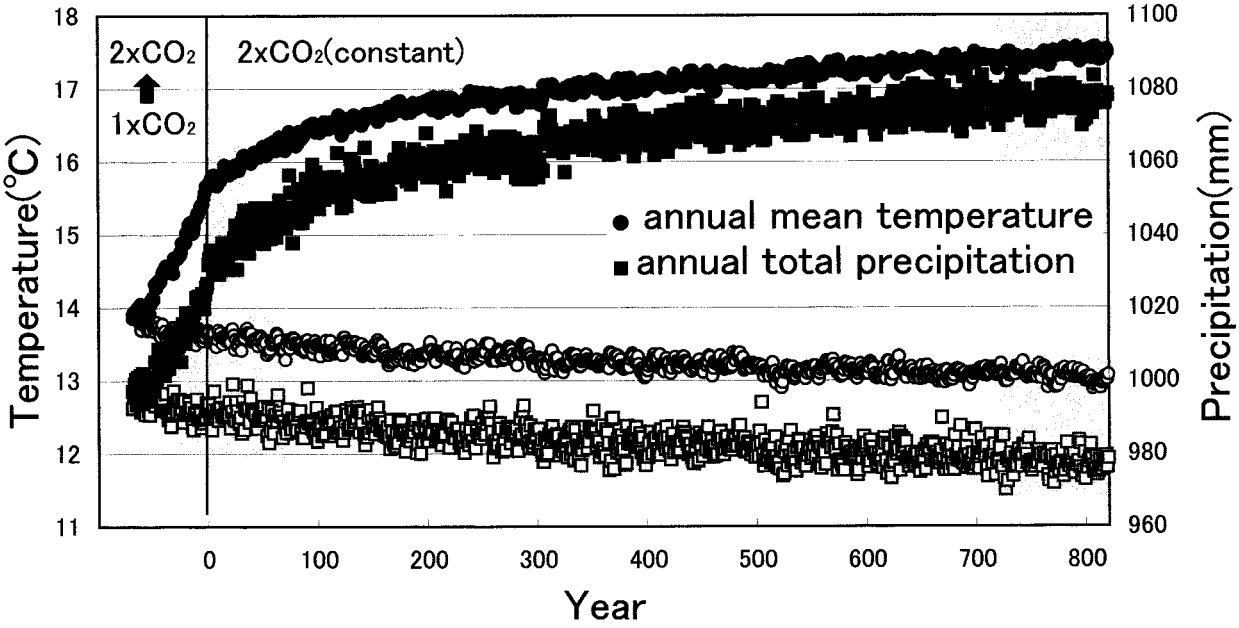

FIG. 1. Time changes of annual total precipitation and annual mean temperature averaged over the globe in the $2 \times CO_2$ run and the control run. Shaded areas indicate those periods for which the differences between the $2 \times CO_2$ run and the control run are described in the text. Note that model year 0 is the time at which the atmospheric carbon dioxide reached doubling.

2. Methodology

The numerical model used here is the Commonwealth Scientific and Industrial Research Organization (CSIRO) coupled model. This model is a comprehensive general circulation model that contains atmospheric, oceanic, sea ice (dynamic–thermodynamic plus leads) and biospheric submodels. The horizontal resolution is about 3.2 lat $\times$ 5.6 long with 9 vertical layers in the atmosphere and 12 vertical layers in the ocean (CSIRO9 R21, version Mk2). This model has been used for global warming assessment by the Intergovernmental Panel on Climate Change (Kattenberg et al. 1996), and in other studies of climate change (Gordon and O'Farrell 1997; Cai et al. 1997). Details of the coupled model components, the spinup methods, and the flux corrections are given in Gordon and O'Farrell (1997).

The coupled model used here is able to simulate the present climate well, with only a small amount of climate drift. The global mean surface air temperature has a long-term cooling trend as shown later in this section. Such a trend is not peculiar to the CSIRO9 R21 model only, and the reasons for the drift have been discussed by Cai and Gordon (1999). The IPCC 1995 report also showed that the CSIRO coupled model simulates the present climate fairly well [see Tables 5.2–5.5 and Figs. 5.1–5.4 in Gates et al. (1996)]. The model has been shown to produce El Niño– and La Niña–like phenomena (Gordon and O'Farrell 1997), although the magnitudes were not large enough and their occurrence frequencies were underestimated, which is symptomatic of a coarse-resolution coupled model. The model has also been found to simulate an abrupt shift in climate similar to one that occurred in the North Pacific around the winter of 1976, and also to other abrupt observed climate changes (Yonetani and Gordon 2001). In a companion model that was run with a slab ocean, the overall patterns of standard deviations of monthly mean surface air temperature were reasonably similar to the observations (Gordon and Hunt 1994). However, the standard deviations of the mean surface air temperature were underestimated over Asia, the eastern Pacific Ocean and a few other areas. The variability over the oceans is improved in the current coupled model compared to the slab ocean model, although still underestimated compared to observations.

In the experiment described here, the coupled model was subject to a 1% compounding CO_2 increase up to $2 \times CO_2$ (70 yr), with the CO_2 being held constant at $2 \times CO_2$ for a further 820 yr. The model year numbering is thus defined as -70 for the start of this run, year 0 at CO_2 doubling, and year numbers 0 to 820 for constant $2 \times CO_2$. The companion control run with the current CO_2 level ($1 \times CO_2$) has the same year numbering (-70 to 820). Figure 1 shows how the globally averaged annual mean surface temperature and annual total precipitation move toward an equilibrium state in the $2 \times CO_2$ run. The mean temperature is just less than 14°C at the start of the transient run, and rises to over 15.5°C at $2 \times CO_2$ (year 0). After that, the mean temperature keeps rising to 16.5°C at year 100, to 17°C at year 350, and reaches almost 17.5°C around year 750. The global mean annual precipitation is enhanced as the global mean temperature rises. The precipitation is about 1000 mm initially, and increases by nearly 30 mm at model

year 0, and by an additional 20 mm by year 100. After year 700, the annual precipitation is nearing stabilization at about 1075 mm.

In the control run, the mean temperature and precipitation exhibit a long-term trend although the changes are slight. The temperature and the precipitation decrease by about 0.5°C and nearly 20 mm during the first 600-yr period, respectively, and appear to have reached a state of near equilibrium after year 550 in the control run. Because both the climates of the $2 \times CO_2$ run and the control run have long-term trends, the changes in climate are assessed as follows. The changes in means and occurrence frequency of extremes due to doubled CO_2 are analyzed by comparing the climatic conditions obtained from 30-yr time series of climatic elements from the $2 \times CO_2$ run with those obtained from a corresponding 100-yr time series during the control run (as a rule). An exception is for the last 100 yr when the globally averaged annual mean surface temperature and annual precipitation are almost in a steady state. For this period, 100 yr of data for both the $2 \times CO_2$ run and the control run are used to identify changes in the equilibrium state due to global warming. The trends in the $1 \times CO_2$ and $2 \times CO_2$ time series are not a major consideration because the magnitudes of the trends for 100 yr in control run and 30 yr in the warmer climate are small in comparison with the differences between the two climate conditions. The effects of this treatment on results are considered in the summary and discussion section.

Changes in the annual and four seasonal values due to doubling of the CO_2 were examined for several periods during the 820-yr run. The season-to-season variation of warming is most noticeable in higher latitudes where the magnitude of the warming is largest in winter. This common feature of global warming has been noted from the earliest stages of climate change simulations (e.g., IPCC 1990). The seasonal variations in the spatial patterns of change for precipitation are not so remarkable as for temperature although precipitation is most enhanced in the intertropical convergence zone in summer. As to long-term variations, the changes were similar in most respects except for the magnitude of change. Thus we will now treat annual mean temperature, seasonal mean temperature for June–August (JJA), and annual total precipitation, and only describe changes for the first 30-yr period and for the last 100-yr period in this paper.

3. Effects of changes in means and standard deviations on occurrence frequency of extremes

In this section, the effects of changes in the mean and variance on the occurrence frequency of extremes are first considered by assuming that the occurrence distributions of the climate elements concerned are normal. Because a normal distribution has been shown for temperature (Mearns et al. 1984), the applicability of the assumption is assessed using statistical considerations based on 100-yr time series at each grid box obtained from the long runs. The purpose of this section is to provide justification for the way in which the extremes are analyzed in the following two sections, and also to allow for a rational interpretation of what the analyses show in the summary.

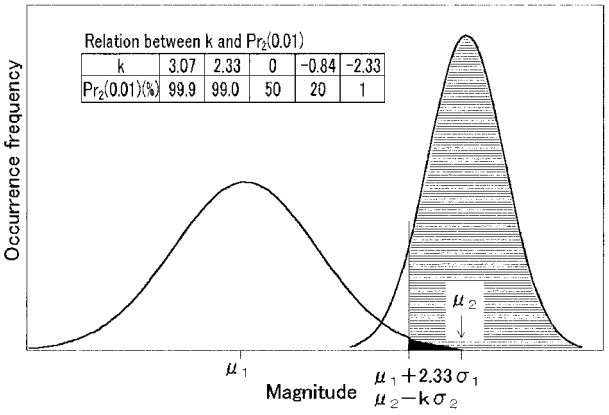

FIG. 2. A schematic representation of changes in occurrence frequency of extremes due to global warming. On the left is a frequency distribution of an element in the $1 \times CO_2$ climate and on the right is an example of the change in mean and frequency distribution that may occur in the $2 \times CO_2$ climate. The solid area marks the 1% high extreme of a normal distribution. The hatched area represents an increase in the number of extreme events in a warmer climate. The relation between k and $Pr_2(0.01)$ is also shown.

Extremes are defined to be values that are larger (smaller) than the maximum (minimum) in 100-yr time series in the $1 \times CO_2$ run in this paper. We now define (μ_1, σ_1) to be the mean and standard deviation of an element, say seasonal mean temperature, in the $1 \times CO_2$ climate, whose occurrence distribution is shown on the left in Fig. 2. If the frequency distribution of such an element has a normal distribution, then a high extreme for which the occurrence probability is less than 1/100 would be higher than $(\mu_1 + 2.33\sigma_1)$. In the $2 \times CO_2$ climate let the corresponding mean and standard deviation be given by (μ_2, σ_2), with a distribution shown schematically on the right in Fig. 2. Considering the overlap in the two occurrence probability distributions, then the occurrence probability that an element in the $2 \times CO_2$ climate exceeds the high extreme in the $1 \times CO_2$ climate [hereafter referred to as $Pr_2(0.01)$] is determined by a parameter k, where k is defined by $(\mu_1 + 2.33\sigma_1) = (\mu_2 - k\sigma_2)$. Since the frequency distribution is represented by a normal distribution, $Pr_2(0.01)$ becomes 99.9% when $k = 3.07$; 50% when $k = 0$; and 20% when $k = -0.84$. [A similar methodology can be used for the occurrence probability of an element in the $2 \times CO_2$ being less than the low extreme $(\mu_1 - 2.33\sigma_1)$].

The parameter k is next shown to comprise two basic parts. One of these is the signal-to-noise ratio, R, which is defined as the ratio of the mean temperature change

to the control run standard deviation, that is, $R = (\mu_2 - \mu_1)/\sigma_1$. It follows that $k = (R - 2.33)\sigma_1/\sigma_2$. Thus the occurrence probability that an element in the $2 \times CO_2$ run exceeds the high extreme in the control run [i.e., $Pr_2(0.01)$] is not only determined by R (which reflects the change in the mean), but also by σ_1/σ_2, which reflects the change in the standard deviation.

In terms of R, the conditions of $\mu_2 = (\mu_1 + 2.33\sigma_1)$, that is, $Pr_2(0.01) = 50\%$, and $(\mu_2 - 3.07\sigma_2) > (\mu_1 + 2.33\sigma_1)$, that is, $Pr_2(0.01) > 99.9\%$, are given by $R = 2.33$, and $R > (2.33 + 3.07\sigma_2/\sigma_1)$, respectively. Thus, when R is larger than 2.33, then the occurrence probability of an extreme is greater than 50%, regardless of the magnitude of σ_2. If the standard deviation in the $2 \times CO_2$ climate is twice as large as that in the $1 \times CO_2$ climate, then the occurrence probability of a high extreme exceeds 99.9% when $R > 8.47$. If it is half as large, then the high extreme occurrence probability becomes larger than 99.9% when $R = 3.87$. The condition that $(\mu_2 + 0.84\sigma_2) = (\mu_1 + 2.33\sigma_1)$, that is, $Pr_2(0.01) = 20\%$, is given by $R = (2.33 - 0.84\sigma_1/\sigma_2)$. Thus, if σ_1/σ_2 is 0.5, the occurrence probability of the high extreme is 20% when $R = 1.91$. If σ_1/σ_2 is 2, then the high extreme occurrence probability becomes 20% when $R = 0.65$.

Because $k = (R - 2.33)\sigma_1/\sigma_2$ and $Pr_2(0.01)$ becomes larger as k becomes larger, it follows that the occurrence probability that an element in the $2 \times CO_2$ climate exceeds the high extreme in the $1 \times CO_2$ climate becomes larger as the difference of the climatic means becomes larger. On the other hand, the effect of σ_2 on the high extreme occurrence probability has a dependence on the sign of $(R - 2.33)$. As σ_2 becomes smaller, k becomes larger when $R > 2.33$ and k becomes smaller when $R < 2.33$. Thus a larger standard deviation leads to a decrease in the extreme occurrence probability (and vice versa) when $R > 2.33$, that is, $Pr_2(0.01) > 50\%$. On the other hand, it leads to an increase in the extreme occurrence probability when $Pr_2(0.01) < 50\%$.

Next a goodness of fit test is undertaken to see how well the distributions of seasonal/annual mean surface air temperature and precipitation fit normal distributions. Two time series for the first and last 100 yr with $1 \times CO_2$ and one time series for the last 100 yr with $2 \times CO_2$ are tested at every gird box. A range between $(\mu - 1.54\sigma)$ and $(\mu + 1.54\sigma)$ is divided into seven equal intervals (i.e., 0.44σ) and cell frequencies are counted at nine categories to be tested, where μ and σ are the mean and standard deviation, respectively. The expected frequencies of categories smaller than $(\mu - 1.54\sigma)$ and larger than $(\mu + 1.54\sigma)$ are lowest and equal to 6.2 per 100 yr.

A chi-square test with a 5% significance level showed that the occurrence distribution of the seasonal mean temperature, and thus the annual mean temperature, is normal at almost all grid boxes in every season for both the $1 \times CO_2$ and the $2 \times CO_2$ climate. There are some exceptions to this, but these are small in size, and are scattered in high latitudes in the Northern Hemisphere (NH) and along 60°S (not shown). On the other hand, the frequency distribution of seasonal precipitation is normal over large areas but there are several regions where the occurrence probability cannot be represented by a normal distribution. These regions include a part of Antarctica and almost all desert areas in the subtropical high-pressure belt. Figure 3 shows the regions where the test indicates that the occurrence frequency of precipitation for JJA for the last 100 yr in the $2 \times CO_2$ run is normal. The areas where the occurrence frequency of seasonal precipitation is not normally distributed is rather wider for JJA and December–February (DJF) than for March–May (MAM) and September–November (SON), but the differences between the four seasons are not very large. Similar figures to Fig. 3 are obtained for all other seasons in both the $1 \times CO_2$ and $2 \times CO_2$ runs. As for the annual total precipitation, its frequency distribution is also not normal in the areas mentioned above, though their dimensions are smaller.

Figure 3 also shows the occurrence number of zero JJA precipitation and the ratio of the kurtosis of the occurrence distribution to that of a normal distribution, that is, 3. The areas where the ratio is larger than 2 are included in the areas where the frequency distribution is not normal, which indicates that the numbers of the occurrence are smaller around the mean and larger off the mean than those for a normal distribution there. The areas where zero precipitation is recorded many times are located in dry regions as well. A similar feature in the pattern of the occurrence frequency of precipitation is also seen in the control run. Thus the warming does not appear to cause much change in the spatial pattern of the frequency distribution showing normality in the current climate.

4. Changes in mean temperature and occurrence frequency of extremes

Changes in the seasonal and annual mean surface air temperatures between the climatic means for $2 \times CO_2$ over 30 yr and for $1 \times CO_2$ over 100 yr just after the year when CO_2 stops increasing (model year 0) are similar to those of other simulations (Kattenberg et al. 1996). A maximum warming is seen in high northern latitudes in all mean temperatures, except for the JJA season, and the warming is largest in the DJF season (Figs. 4a,b). There is a minimum warming around Antarctica and in the northern North Atlantic, with the latter area even showing a region of cooling in DJF. Fluctuations of the mean temperatures are small over the oceans at low latitudes and large at high latitudes, and the seasonal mean temperature fluctuates more than the annual mean temperature, with the greatest variation being at high latitudes in the winter. The simulated pattern of the standard deviation of the annual mean temperature, ranging from 0.2°C to more than 1.2°C, is in general agreement with the observations, and is similar

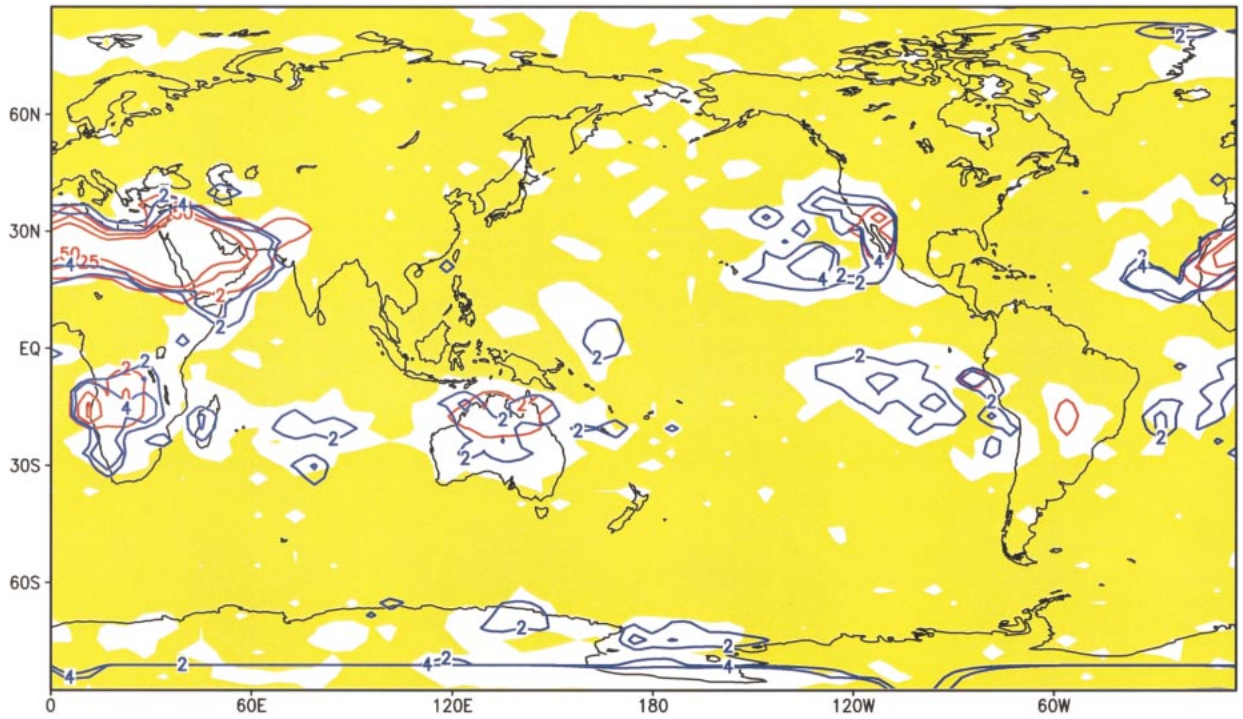

FIG. 3. Regions where the chi-square test indicates that the frequency distribution of seasonal total precipitation for JJA is normal (colored yellow). Red lines indicate the number of occurrence of zero amount (2, 25, 50) and blue lines the ratio of the kurtosis of the occurrence distribution to that of normal distribution (2, 4 only).

to that reproduced in other models (Hansen et al. 1988; Stouffer et al. 1994; Manabe and Stouffer 1996). Here it is worth noting that the geographical distributions of the standard deviations of mean temperatures in the control run do not undergo significant time variations (see Figs. 4a,b and Figs. 5a,b).

Over the oceans in the Tropics, where the standard deviation of the annual mean temperature is less than 0.2 for most of the area (and over wide areas in DJF), the magnitude of the warming is less than 2°C as a whole. However, there are areas where rise of the temperature is over 2°C, and these areas are located in the eastern tropical Pacific where the standard deviation is larger than 0.2°C (Figs. 4a and 4b). Thus there are indications of an El Niño–like temperature response as has been reported for other models (Knutson and Manabe 1995, 1998; Meehl and Washington 1996; Timmermann et al. 1999).

Changes in interannual variability due to the warming are different according to region (not shown); temperature variability increases in some areas and decreases in the other areas as reported previously [Figs. 7 and 8 in Gordon and Hunt (1994)]. The ratio of the standard deviation in the $2 \times CO_2$ climate run to that in the control run lies between 0.6 and 1.4 over most of the globe for all seasons. According to the *F* test, the two samples are statistically different at the 0.01 significance level if the ratio between the standard deviations is larger (smaller) than 1.6 (0.6) when samples sizes are 100. There are some areas where the ratio is less than 0.6. Exceptions are the Arctic Ocean and around the Antarctic continent in JJA and the Sea of Okhotsk, the Labrador Sea, and the Norwegian Sea in DJF. These regions are located where the quite variable air temperatures over sea ice have been replaced by much less variable air temperatures over the seawater (the latter remaining close to the freezing point of seawater). Similar results have been obtained in other coupled model simulations [Fig. 12 in Cao et al. (1992)].

Because the magnitude of the change in temperature is much larger than the standard deviation in many regions, the extreme high temperatures that occur in the control run are recorded very often in the $2 \times CO_2$ run. This tendency is most outstanding in the low latitudes where the ratio of rise of the temperature to standard deviation in the control run, that is, *R*, is largest (over 5.4) and is most pronounced for the annual mean temperature (Figs. 4c and 4d). The annual mean temperature in the $2 \times CO_2$ run is always higher than the maximum achieved during the control run in low and middle latitudes, and record-breaking high temperatures are produced more than 15 times during 30 yr in the $2 \times CO_2$ run in most high latitudes (Fig. 4c). The warming is largest in the high northern latitudes in DJF (Fig. 4b), but the chance occurrence of the extreme high temperatures in the NH is not as great in that season (Fig. 4d) as it is in other seasons (Fig. 4c). For example, north of 60°N where the warming is noticeable (more than

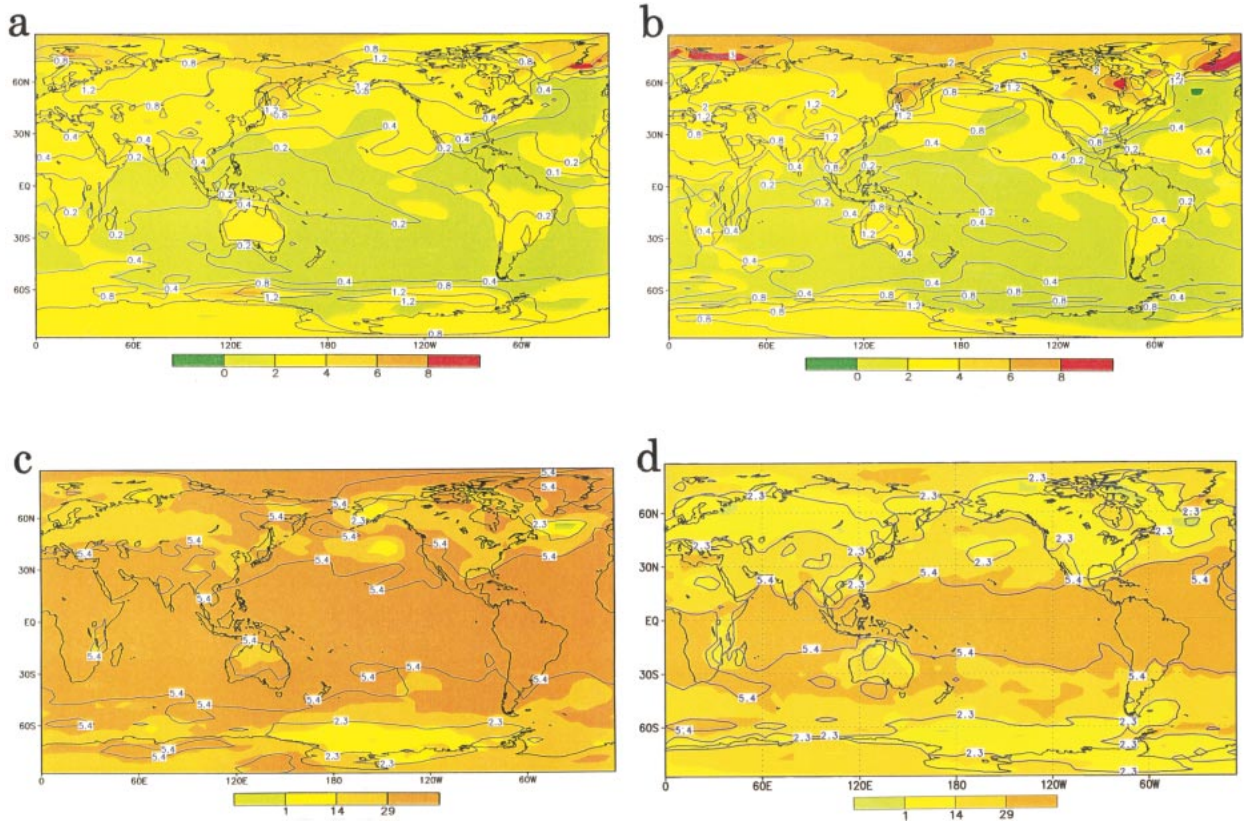

FIG. 4. Geographical distributions of surface temperature statistics for (a, c) the annual mean and for (b, d) DJF for the 30-yr period just after the atmospheric carbon dioxide has doubled. Displayed in (a) and (b) are the changes in the temperatures averaged over 30 yr in the $2 \times CO_2$ run, together with the standard deviation in the control run (contour lines), in units of °C. Displayed in (c) and (d) are the number of cases when the temperature in the $2 \times CO_2$ run exceeds the maximum temperature of the corresponding 100-yr time series in the control run. Contour lines show the ratio of the rise in the temperature to the control run standard deviation, i.e., *R*. The areas coloured orange in c and d are areas where the temperature in the $2 \times CO_2$ run is always higher than the maximum in the control run.

4°C in most areas), and the standard deviation is large in the control run (more than 2°C in most areas), the occurrence probability of an extremely high temperature is less than 15/30 over wide areas in DJF.

From the discussion in the previous section, it can be expected that the occurrence frequency of a high extreme of temperature during a 30-yr period is less than 15 and larger than 29.97 in the areas where $R < 2.3$ and $R > 5.4$, respectively, assuming $\sigma_1/\sigma_2 = 1$. Figure 4 shows that the expected relations between the occurrence frequency of the high extreme and *R* are almost satisfied for both the annual mean and DJF mean temperatures although σ_1/σ_2 varies from 0.6 to 1.4 as described the above. Thus, it is indicated that changes in the climate mean temperature play a more important role in the occurrence of extremes than do changes in the standard deviation.

During the increase in atmospheric CO_2 concentration, the temperature rises most noticeably in high northern latitudes (Fig. 4). Warming after the atmospheric CO_2 stops increasing then becomes most noticeable in high southern latitudes, especially around the Antarctic continent. The increase in annual mean temperature exceeds 6°C for areas south of 60°S and north of 60°N when the $2 \times CO_2$ climate is in an almost steady state (Fig. 5a). The warming of the DJF mean temperature is most noticeable in high northern latitudes and not as much in high southern latitudes (Fig. 5b). From the difference between changes of annual mean and DJF mean temperatures in northern and southern high latitudes, it follows that the high-latitude warming is largest in the winter season for both hemispheres. A noticeable warming is also seen in the northern North Atlantic Ocean as well as around the Antarctic continent where deep convection and large-scale vertical motions occur in the present climate. Thus the interhemispheric asymmetry of warming is progressively eliminated, although an ocean–land asymmetry remains. Over the tropical Pacific, an El Niño–like response is still evident.

The occurrence probabilities of high extremes of temperature become larger as the warming advances. In the last 100-yr period, the change (increase) in the climate annual mean temperature is larger than 5.4 times the standard deviation in the control run, and the occurrence frequency of extremes becomes 100 100 yr^{-1} for most parts of the globe (Fig. 5c). Similar changes are found

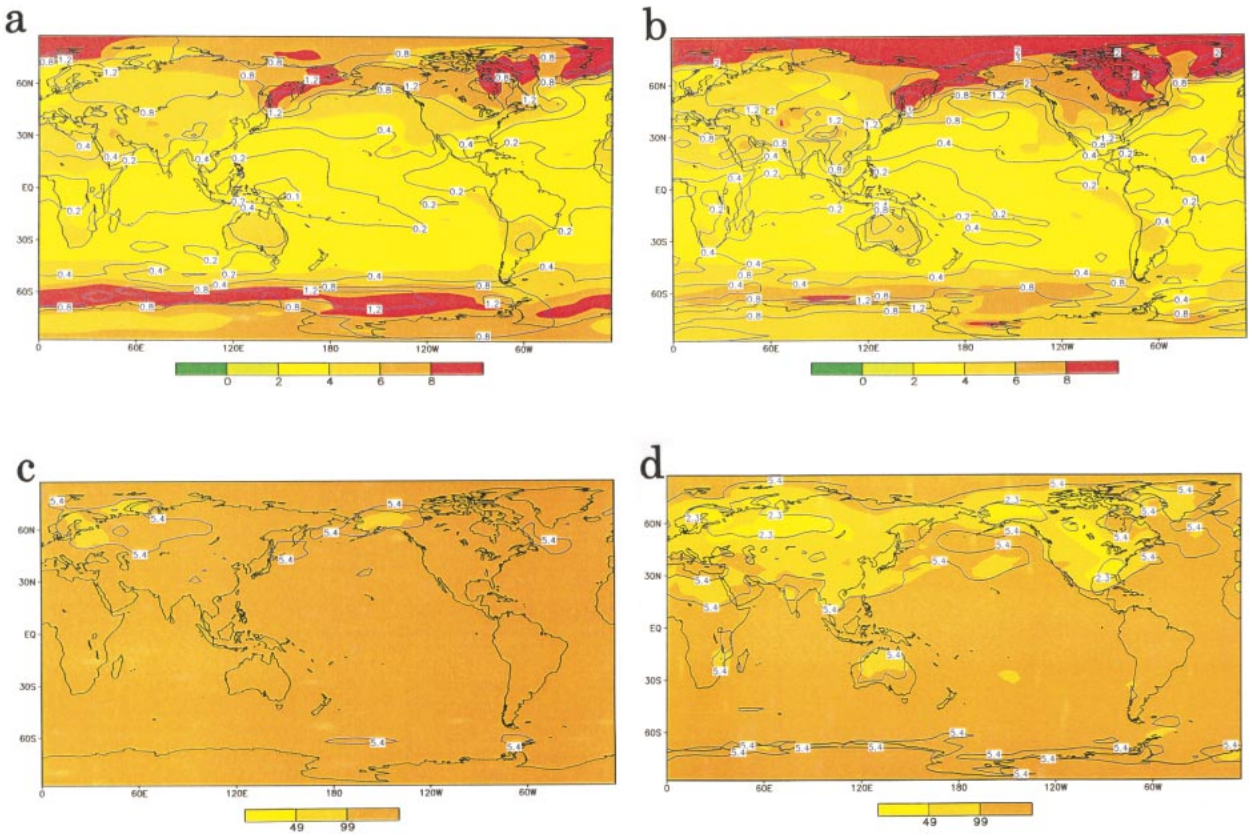

FIG. 5. The same as in Fig. 4 but for a 100-yr period starting at model year 720.

in the occurrence frequency of high extremes in the DJF mean temperature, but not as much as for the annual mean temperature. The main regions where the occurrence probability does not become as high as 1 are the continental areas of the NH, and in parts of Australia in the Southern Hemisphere (Fig. 5d). Over a few regions in the continents of the NH where R is less than 2.3, the occurrence frequency of the high extreme is less than 50. The expected relationships between R and the occurrence frequency of high extremes are thus confirmed.

5. Changes in precipitation and occurrence frequencies of their extremes

Although global warming enhances the global mean precipitation (Fig. 1), there can be either increased or decreased precipitation at the regional scale. Precipitation mainly increases in the high latitudes and over the oceans in the Tropics. Regional changes in the annual total precipitation just after CO_2 doubling are shown in Fig. 6a, and these results are essentially in common with a number of other results (Kattenberg et al. 1996). The partial changes in precipitation evident by about model year 15 become increasingly more noticeable as global warming develops. By model year 750, the global warming enhances annual precipitation by almost 100 mm in high latitudes, and by more than 300 mm in some regions over the oceans in the Tropics. On the other hand, the annual precipitation decreases by more than 100 mm in some areas in the Middle East, Africa, and Australia (Fig. 6b). During the course of the increased CO_2 run, there was a gradual enhancement of the decrease in rainfall amount for these regions. However, it is interesting to note that there was a strong initial decrease in the Middle East compared to the other two regions. Thus, in general, it is apparent that the model climate has a tendency for the precipitation amounts to continue to increase or decrease during the course of model climate shift toward its equilibrium state.

The increase in the precipitation in the high northern latitudes can be attributed to enhanced water vapor convergence in that region (Manabe and Wetherald 1975). The model employed here also shows that areas where precipitation increases (decreases) are coincident with where changes in the water vapor transport imply an enhancement of the horizontal convergence (divergence) of moisture at low levels, and there is a clear link between them (Figs. 6a and 6b). There is also an El Niño-like response in the precipitation and wind fields in the equilibrium state. The annual total precipitation increases over the central and eastern tropical

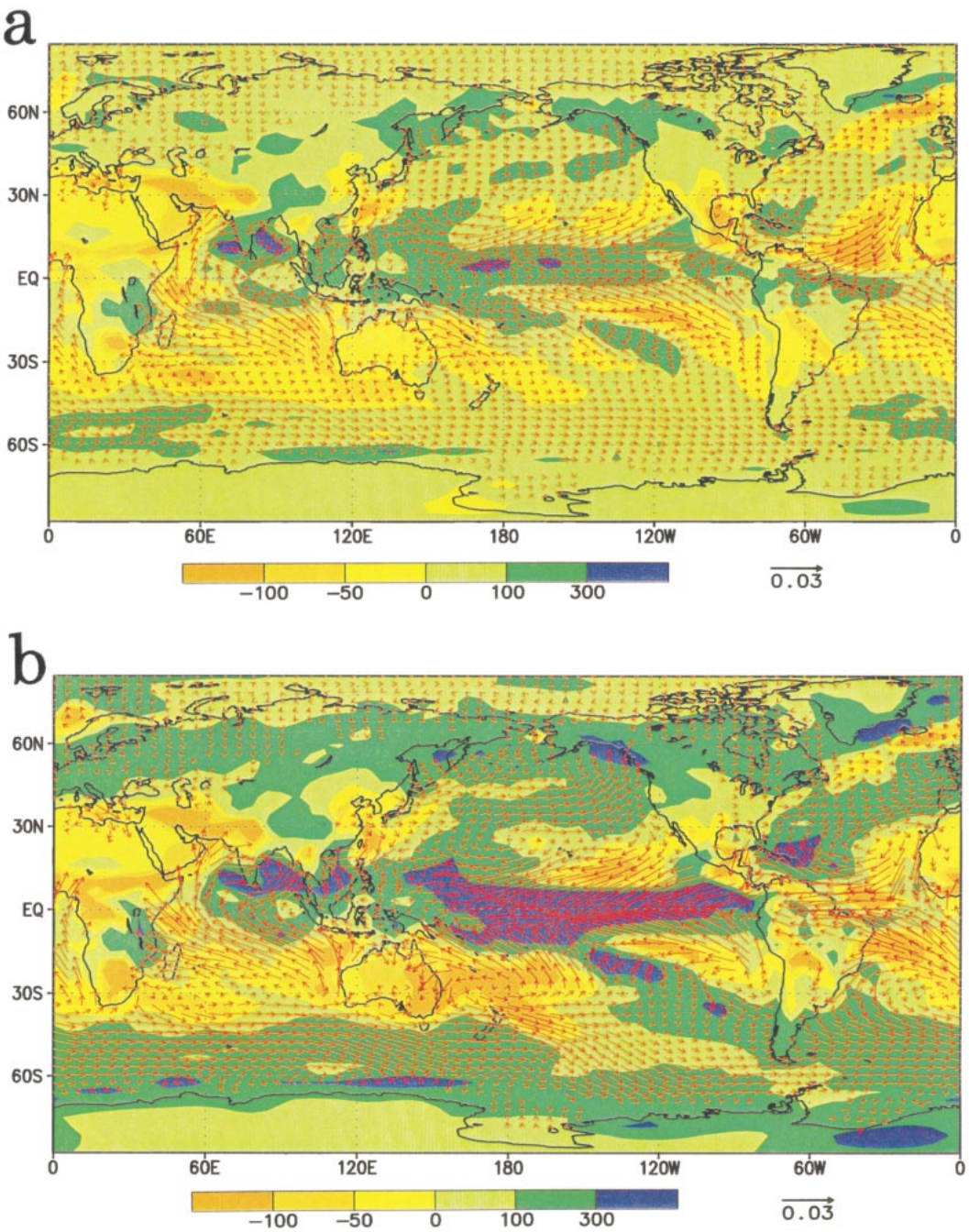

FIG. 6. Geographical distributions of changes in the annual precipitation (in units of mm) and changes in the mean water vapor transport at 980-hPa level. These are for (a) model years 0–29 and for the 100-yr period covering (b) model years 720–819.

Pacific and decreases over most of the tropical Atlantic and African regions. Changes in the wind field show that the trade winds weaken over the western half of the tropical Pacific (not shown). This can be inferred from changes in the mean water vapor transport, which show an enhancement of the westerly component of the winds over the western tropical Pacific (Fig. 6b).

With regard to the standard deviation of annual precipitation or seasonal precipitation, it is difficult to identify a significant change during the early stages of the transient run, as has been reported elsewhere (Rind et al. 1989). The ratio of the standard deviation in the 2 $\times$ CO_2 climate run to the control run lies between about 0.6 and 1.6 for wide areas. There are some areas where the variation changes significantly (the ratio is larger than 1.6 or smaller than 0.6) due to global warming

though their extent is not large and there is not much spatial structure. The geographical distribution of the ratio varies widely from region to region and has many small-scale features. The year-to-year variability generally change with the same sign as the mean precipitation itself as has been previously shown (Rind et al. 1989).

In areas where precipitation is enhanced, the occurrence number of high extremes being more than the maximum during a 100-yr period in the control run becomes larger as the $2 \times CO_2$ run progresses, and a similar change is brought about in areas where the precipitation decreases (Figs. 7a,b). As the annual total precipitation continues to increase or decrease at the regional scale after model year 0, the occurrence probability of a high extreme or a low extreme becomes larger in each case. Record-breaking abundance or deficit of precipitation occurs in more than 5 yr out of 30 only in small areas when CO_2 has just attained doubling. By model year 750, the occurrence probability of high extremes and low extremes exceeds 19/100 in those regions where the precipitation increases and decreases noticeably, respectively. The areas where the occurrence frequency of a high extreme is not less than 20/100 is coincident with the area where the ratio of the mean precipitation increment to the control run standard deviation is larger than 1.5, which is the expected value from the theoretical considerations. On the other hand, the areas where the occurrence frequency of low extremes exceeds 19/100 include where the ratio of the mean precipitation decrease to the standard deviation is more than 1.5. This indicates that the changes in precipitation have had a pronounced effect on the occurrence of extremes in dry areas. Here it is worth noting that there are areas where the occurrence frequency of low extremes is zero in Sahara Desert. This is caused by the low extreme being zero in these areas in the control run and by the number of years when annual total precipitation is zero increasing in the $2 \times CO_2$ climate run though this is not so noticeable as for JJA (Fig. 3).

Figure 8 shows an example of the link between R, σ_1/σ_2, and the occurrence frequency of high and low extreme JJA total precipitation during a 100-yr period around model year 750. In spite of the fact that the occurrence frequency is not represented by a normal function for large areas (see Fig. 3) and warming brings about a considerable change in the standard deviation in some regions (not shown but $0.6 < \sigma_1/\sigma_2 < 1.6$ for large areas in the same way as for annual total precipitation), a proportional relationship is still formed. The occurrence frequency of the high extreme exceeds 40 (80) out of 100 when R is larger than 2.5 (5), and when R is less than -2.5 the occurrence frequency of the low extreme exceeds 60.

The link between the occurrence frequency and R is in accord with the results from the theoretical considerations (section 3) when R is positive, but the link is slightly different from the theoretical results when R is negative. There are cases when the occurrence frequency of the low extreme is more than 50 despite that R is not small enough, that is, $-2 < R < 0$. A large change in the occurrence frequency of the low extreme is caused by a small change in R at grid boxes where the occurrence frequency of the low extreme exceeds about 40. Figure 8 shows that the occurrence frequency of the low extreme is large while the value of R is apparently not large enough, and this happens at grid boxes where the ratio of kurtosis to that of a normal distribution is larger than 2 in dry regions (Fig. 3). The kurtosis becomes large when the occurrence frequency is relatively small around the mean and large off the mean. This means that the standard deviation in the $1 \times CO_2$ run is calculated to be large (R becomes small) for cases of large kurtosis, and the occurrence frequency number of the low extreme becomes large when kurtosis is large in the $2 \times CO_2$ run. Thus Fig. 8 also shows that larger (smaller negative) R indicate a larger occurrence probability of the high (low) extreme even if the occurrence frequency distribution is not normal so long as the kurtosis of the distribution is larger than that of a normal distribution.

6. Summary and discussion

A multiple century simulation using a coupled ocean–atmosphere model demonstrates characteristic spatial patterns of climate change and changes in extremes due to global warming with regard to seasonal and annual values of surface air temperature and precipitation. It was found that global warming induces an El Niño–like change in low latitudes, which a few other coupled models have previously shown (Knutson and Manabe 1995, 1998; Meehl and Washington 1996; Timmermann et al. 1999). Another characteristic regional change projected is that of a decrease in precipitation in the dry regions of the current subtropical high-pressure belts despite an increase in global mean precipitation. The contrast between dry areas and wet areas in general becomes more striking as time advances after CO_2 has attained doubling. This suggests that global warming enhances the atmospheric circulation without changing its pattern in low and middle latitudes except for over the tropical Pacific Ocean where an El Niño–like response is detected.

The coupled model used here displays an initial interhemispheric asymmetry in warming, which has been seen in other CO_2 increase simulations (IPCC 1992; Kattenberg et al. 1996). The surface air temperature increases much more rapidly in the northern high latitudes, except for northern North Atlantic, than in the southern high latitudes during the CO_2 concentration increase. However, it is shown that the asymmetry of warming disappears except for an ocean–land asymmetry when the climate system attains its equilibrium state. The asymmetric warming in high latitudes when

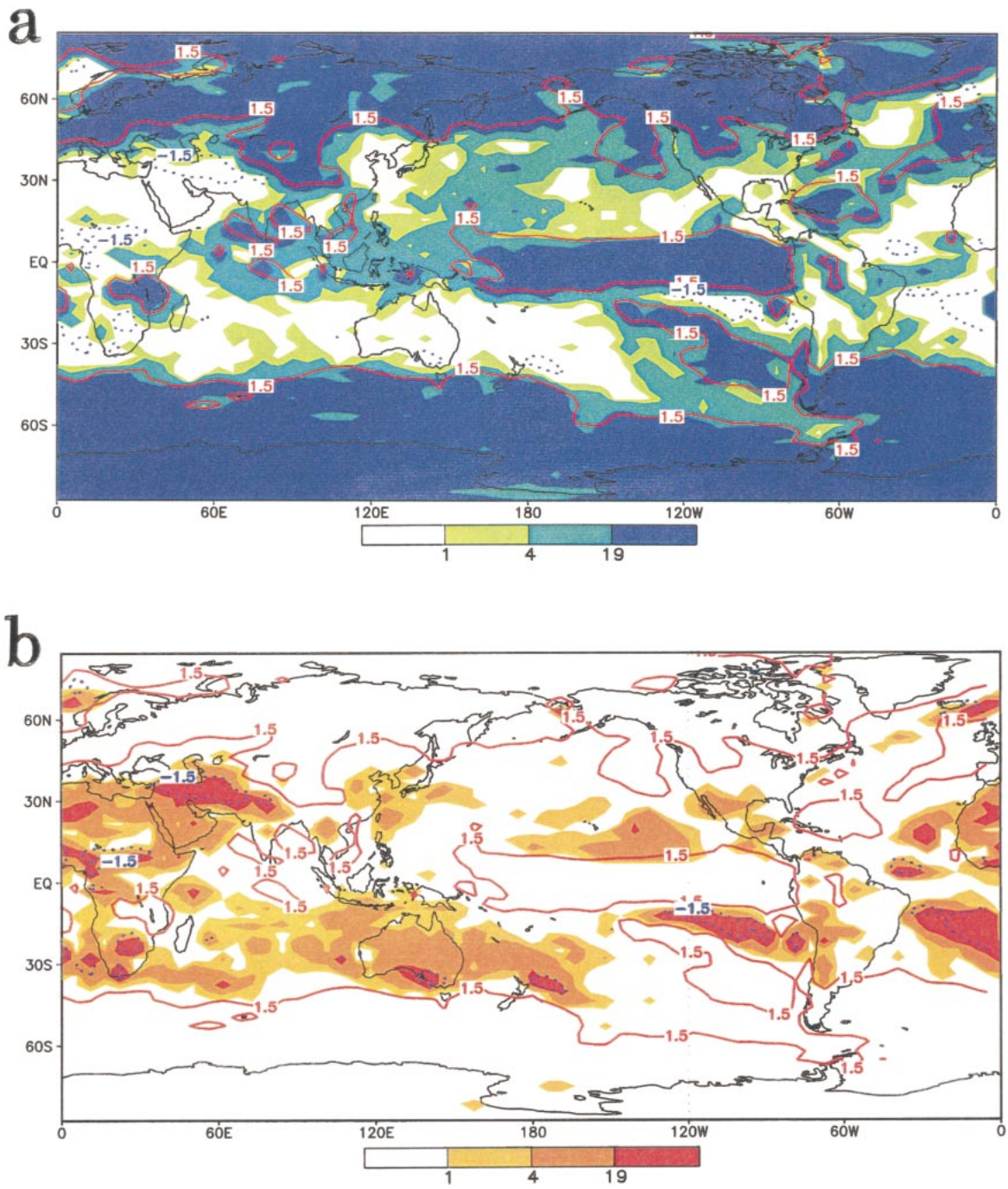

FIG. 7. Geographical distribution of the number of years when the annual precipitation in the 2 × CO_2 run exceeds the maximum in the control run for the last (a) 100 yr, and (b) the same as (a) but for the minimum of the annual precipitation. Also shown by contour lines (intervals of 1.5) is the ratio of the precipitation changes to the standard deviation in the control run.

CO_2 is doubled is associated with the thermal inertia of the oceans due to deep convection and large-scale vertical motions at high latitudes. The implied effective heat capacity, however, is considered to become smaller as the thermohaline circulation weakens in the warmer climate (Manabe and Stouffer 1993, 1994; Gordon and O'Farrell 1997; Stocker and Schmittner 1997; Cai and Gordon 1998; Schmittner and Stocker 1999; Wood et al. 1999).

The globally averaged annual mean surface temperature becomes 4.5°C warmer in the 2 × CO_2 run than the control run at around model year 800 (Fig. 1). The global mean annual precipitation is nearing stabilization at 1075 mm, which is a 10% increase. These increments

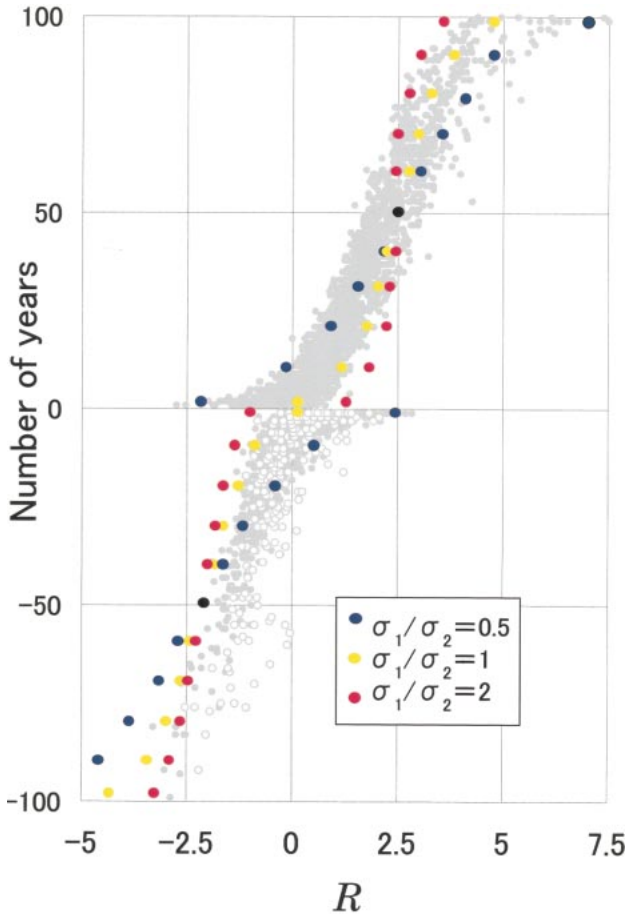

FIG. 8. The relation between R (the ratio of the magnitude of the change of the climate mean precipitation to the standard deviation in the control run) and the number of years when the precipitation in the $2 \times CO_2$ run (last 100 yr) exceeds the maximum precipitation in the control run. Dot points above the axis (positive numbers of years) show the number of years when this occurs per grid point for the JJA total precipitation. Dot points below the axis (negative numbers of years) are for the number of years per grid point when the precipitation in the $2 \times CO_2$ run is smaller than the minimum value in the control run. Open circles are for grid boxes where the ratio of kurtosis is larger than 2 in the $1 \times CO_2$ run or/and the $2 \times CO_2$ run. The theoretical relations are also shown when a normal distribution is assumed (coloured circles).

are consistent with the equilibrium changes in the temperature and the precipitation obtained when the CSIRO atmospheric model was coupled to a mixed layer ocean model having an average depth of about 70 m (Watterson et al. 1997; Watterson 1998). In the latter mixed layer ocean coupled model, it took about 35 yr for the climate system to reach an approximate equilibrium state. This is considerably shorter than the 700 yr taken to reach equilibrium in the current coupled atmosphere–ocean general circulation model. This is indicative that the effective heat capacity of the ocean decreases gradually and becomes similar to that of the mixed layer ocean model used above.

The asymmetry in warming not only depends on the presence of convection and overturning in the ocean, but is also subject to feedback processes. If there are perturbations that cause a change in overturning, then several feedbacks (positive and negative) come into play as described in Cai and Gordon (1999). In the case of the current coupled model with increasing CO_2, there is a positive feedback between decreased overturning and the warming due to external forces. Once the overturning weakens during the course of the warming, the warming is enhanced at regional scales because the weakened overturning leads to a decrease in effective heat capacity. This works to weaken the overturning since the warming of the surface layers increases the static stability of the ocean if it is not accompanied by an increase of salinity. There is in fact a freshening at high latitudes caused by increased precipitation over evaporation, increased land runoff, and ice melt (Gordon and O'Farrell 1997). Thus as the overturning weakens during the warming process, the temperature increase will become more prominent in the high-latitude regions, which showed less warming initially. It has been shown that it would take some centuries for the surface temperature in high-latitude oceans to attain an equilibrium state because the thermohaline circulation needs that amount of time to reach a steady state (Manabe and Stouffer 1993; Schmittner and Stocker 1999). In addition to the above example of a positive feedback, there can also be negative feedbacks. For example, the slowdown in the meridional overturning implies that there is a reduced poleward advection of warm subtropical water (Murphy and Mitchell 1995). Detailed analyses beyond the scope of this paper are needed to draw definitive conclusions regarding the effects of the reduction in overturning on regional temperature changes.

As to changes in extremes of seasonal/annual values, it is shown that the global warming under $2 \times CO_2$ conditions leads to record-breaking high annual and seasonal surface air temperatures becoming common. In addition, record-breaking high or low precipitation amounts often occur. With regard to precipitation changes, it is mainly changes in the annual total that have been addressed in this paper. However, the seasonal total precipitation also undergoes similar changes. The occurrence probability of high extremes in each season becomes larger in high latitudes, and also for broad areas in the oceans in the Tropics. The same changes occur for low extremes in some already drought prone areas such as the Middle East, much of Africa, and Australia.

It is shown that the occurrence probability of extremes in the $1 \times CO_2$ climate can be calculated by two ratios when the occurrence frequency can be represented by normal function. These are the ratio of the magnitude of the change of the climate mean to the standard deviation in the $1 \times CO_2$ climate, R, and the ratio of the standard deviation in the $1 \times CO_2$ to that in the $2 \times CO_2$, σ_1/σ_2. Our numerical experiments show that for temperature R has values ranging to much larger than 5 for large parts of the globe, for precipitation R has

values in the range $-4 < R < 8$, and $0.5 < \sigma_1/\sigma_2 < 2$ for both elements. The numerical experiment shows that R vitally affects the occurrence probability of extremes even for seasonal and annual precipitation whose occurrence distributions are not normal over wide areas. This means that the magnitude of the shift in the climatic mean relative to σ_1 is so large that the effects of other factors on the occurrence probability of the extremes become small. In the analysis it should be noted that long-term trends were not taken into consideration when the standard deviation and occurrence frequencies of the extremes were calculated. The facts described above suggest that almost the same results would have been obtained if the datasets had been detrended.

The occurrence probability for a high extreme of temperature is shown to be 1 in the Tropics at the time of CO_2 doubling and thereafter. This is due to R being largest over the oceans in the Tropics. The standard deviations of the observed annual mean surface temperature are from 0.2° to 0.4°C and more than 1.0°C for wide areas over oceans in the Tropics and high latitudes in the NH, respectively (Jones et al. 1991). Thus if the annual mean temperature increases in the tropical regions by 1°C then R becomes 2.5–5 and the occurrence probability of high extremes becomes about 50%–99%. (This is satisfied when $2.33 < R < 4.66$ if $\sigma_1/\sigma_2 = 1$; $2.33 < R < 6.99$ if $\sigma_1/\sigma_2 = 0.5$; and $2.33 < R < 3.50$ if $\sigma_1/\sigma_2 = 2$, see Fig. 8). On the other hand, the occurrence probability does not exceed 99% in Alaska where the observed standard deviation is about 1.2°C unless the annual mean temperature increases by about 5°C or more.

It has been shown that sulphate aerosols may exert considerable radiative forcing on the atmosphere and may reduce the warming due to increases of greenhouse gas at regional scales. It has been reported that the effects of aerosols are most noticeable in the middle latitudes of the NH and that the maximum winter warming in high northern latitudes becomes less (Kattenberg et al. 1996). Numerical simulations using climate model including aerosol forcing have projected temperature increments of more than 1°C and less than 5°C in most parts of the Tropics and northern high latitudes, respectively [Fig. 4d in Mitchell et al. (1995) and Fig. 3 in Meehl et al. (1996)]. Another has shown temperature increments of less than 1°C for a large part of the globe and negative areas in the high northern latitudes [Fig. 1f in Taylor and Penner (1994)]. It follows that the occurrence probability of a high extreme may become largest over the tropical oceans if the above projections about the high-latitude cooling effects of aerosols are correct. Thus, it is concluded that the occurrence frequency of extreme high values in annual mean temperature in the Tropics might be a better indicator of global warming than the winter mean temperature increment in the high northern latitudes.

An essentially similar change in the occurrence frequency of extremes is suggested to occur for changes in precipitation due to global warming. The occurrence probability of high and low extremes should increase in proportion to the ratio of the absolute difference of climate means to the standard deviation in the $1 \times CO_2$ climate. However, it is difficult to assess validity of this result because the precipitation records are not long enough and there is insufficient spatial coverage to obtain reliable standard deviations globally. Thus, the changes in the occurrence frequency of precipitation extremes derived here should be interpreted with caution. The results show however that the parameter R is a good index for the occurrence probability of the extremes. They also show that the occurrence frequency of a high (low) seasonal/annual precipitation with a 100-yr return period would be more than 20 times 100 yr^{-1} when the climate mean increases (decreases) by more than about 1.5 times the standard deviation.

The results here indicate that the seasonal/annual mean temperature change due to a doubling of CO_2 may become so large that extreme high temperatures in the $1 \times CO_2$ climate may become the norm in the warmer climate. Extreme high or low seasonal/annual precipitation amounts in the current climate are projected to be recorded with considerably enhanced frequency. The results here imply not only that the climate in the doubled CO_2 world will be significantly warmer with greater global mean precipitation, but that there will be significant changes in the frequency of extremes, and that these changes will have considerable impacts on society and the environment.

Acknowledgments. The authors wish to thank two anonymous reviewers for constructive comments. This work was supported by the Science and Technology Agency, Japan (T.Y), and by the Australian Federal Government through the Department of Environment, Sports, and Territories (H.B.G).

REFERENCES

Beersma, J. J., K. M. Rider, G. J. Komen, E. Kaas, V. V. Kharin, 1997: An analysis of extra-tropical storms in the North Atlantic region as simulated in a control and $2 \times CO_2$ time-slice experiment with a high-resolution atmospheric model. *Tellus,* **49A,** 347–361.

Bengtsson, L., M. Botzet, and M. Esch, 1996: Will greenhouse gas-induced warming over the next 50 years lead to higher frequency and greater intensity of hurricanes? *Tellus,* **48A,** 57–73.

Cai, W., and H. B. Gordon, 1998: Transient responses of the CSIRO climate model to two different rates of CO_2 increase. *Climate Dyn.,* **14,** 503–516.

——, and ——, 1999: Southern high-latitude ocean climate drift in a coupled model. *J. Climate,* **12,** 132–146.

——, J. Syktus, H. B. Gordon, and S. P. O'Farrell, 1997: Response of a global coupled ocean–atmosphere–sea ice climate model to an imposed North Atlantic high-latitude freshening. *J. Climate,* **10,** 929–948.

Cane, M. A., A. C. Clement, A. Kaplan, Y. Kushnir, D. Pozdnyakov, R. Seager, S. E. Zebiak, and R. Murtugudde, 1997: Twentieth-century sea surface temperature trends. *Science,* **275,** 957–960.

Cao, H. X., J. F. B. Mitchell, and J. R. Lavery, 1992: Simulated diurnal range and variability of surface temperature in a global

climate model for present and doubled CO_2 climates. *J. Climate,* **5,** 920–942.
Carnell, R. E., and C. A. Senior, 1998: Changes in mid-latitude variability due to greenhouse gases and sulphate aerosols. *Climate Dyn.,* **14,** 369–383.
Colombo, A. F., D. Etkin, and B. W. Karney, 1999: Climate variability and the frequency of extreme temperature events for nine cities across Canada: Implications for power usage. *J. Climate,* **12,** 2490–2502.
Druyan, L. M., P. Londergan, and T. Eichler, 1999: A GCM investigation of global warming impacts relevant to tropical cyclone genesis. *Int. J. Climatol.,* **19,** 607–617.
Gates, W. L., and Coauthors, 1996: Climate models—Evaluation. *Climate Change 1995,* J. T. Houghton, L. G. Meira Filho, B. A. Callander, N. Harris, A. Kattenberg, and K. Maskell, Eds., Cambridge University Press, 229–284.
Giorgi, F., L. Mearns, S. Shields, and L. McDaniel, 1998: Regional nested model simulations of present day and $2 \times CO_2$ climate over the central Great Plains of the United States. *Climatic Change,* **40,** 457–493.
Gordon, H. B., and B. G. Hunt, 1994: Climatic variability within an equilibrium greenhouse simulation. *Climate Dyn.,* **9,** 195–212.
——, and S. P. O'Farrell, 1997: Transient climate change in the CSIRO coupled model with dynamic sea-ice. *Mon. Wea. Rev.,* **125,** 875–907.
——, P. H. Whetton, A. B. Pittock, A. M. Fowler, and M. R. Hyalock, 1992; Simulated changes in daily rainfall intensity due to the enhanced greenhouse effect: Implications for extreme rainfall events. *Climate Dyn.,* **8,** 83–102.
Gregory, J. M., and J. F. B. Mitchell, 1995: Simulation of daily variability of surface temperature and precipitation over Europe in the current and $2 \times CO_2$ climates using the UKMO climate model. *Quart. J. Roy. Meteor. Soc.,* **121,** 1451–1476.
Groisman, P. Ya., and Coauthors, 1999: Changes in the probability of heavy precipitation: Important indicators of climatic change. *Climatic Change,* **42,** 243–283.
Hansen, J., I. Fung, A. Lacis, D. Rind, S. Lebedeff, R. Ruedy, and G. Russell, 1988: Global climate changes as forecast by Goddard Institute for Space Studies three-dimensional model. *J. Geophys. Res.,* **93** (D8), 9341–9364.
Hennessy, K. J., and A. B. Pittock, 1995: Greenhouse warming and threshold temperature events in Victoria, Australia. *Int. J. Climatol.,* **15,** 591–612.
——, J. M. Gregory, and J. F. B. Mitchell, 1997: Changes in daily precipitation under enhanced greenhouse conditions. *Climate Dyn.,* **13,** 667–680.
IPCC, 1990: *Climate Change: The IPCC Scientific Assessment.* J. T. Houghton, G. J. Jenkins, and J. J. Ephraums, Eds., Cambridge University Press, 365 pp.
——, 1992: *Climate Change 1992: The Supplementary Report to the IPCC Scientific Assessment.* J. T. Houghton, B. A. Callander, and S. K. Varney, Eds., Cambridge University Press, 198 pp.
Jones, P. D., T. M. L. Wigley, and G. Farmer, 1991: Marine and land temperature data sets: A comparison and a look at recent trends. *Greenhouse-Gas-Induced Climatic Change: A Critical Appraisal of Simulations and Observations,* M. E. Schlesinger, Ed., Elsevier, 153–172.
——, E. B. Horton, C. K. Folland, M. Hulme, D. E. Parker, and T. A. Basnett, 1999: The use of indices to identify changes in climatic extremes. *Climatic Change,* **42,** 131–149.
Kattenberg, A., and Coauthors, 1996: Climate models—Projections of future climate. *Climate Change 1995,* J. T. Houghton, L. G. Meira Filho, B. A. Callander, N. Harris, A. Kattenberg, and K. Maskell, Eds., Cambridge University Press, 285–357.
Katz, R. W., and B. G. Brown, 1992: Extreme events in a changing climate: Variability is more important than averages. *Climatic Change,* **21,** 289–302.
Katzfey, J. J., and K. L. McInnes, 1996: GCM simulation of eastern Australian cutoff lows. *J. Climate,* **9,** 2337–2355.
Knutson, T. R., and S. Manabe, 1995: Time-mean response over the tropical Pacific to increased CO_2 in a coupled ocean–atmosphere model. *J. Climate,* **8,** 2181–2199.
——, and ——, 1998; Model assessment of decadal variability and trends in the tropical Pacific Ocean. *J. Climate,* **11,** 2273–2296.
——, and R. E. Tuleya 1999: Increased hurricane intensities with CO_2-induced warming as simulated using the GFDL hurricane prediction system. *Climate Dyn.,* **15,** 503–519.
——, ——, and Y. Kurihara, 1998: Simulated increase of hurricane intensities in a CO_2-warmed climate. *Science,* **279,** 1018–1020.
Krishnamurti, T. N., R. Correa-Torres, M. Latif, and G. Daughenbaught, 1998: The impact of current and possibly future sea surface temperature anomalies on the frequency of Atlantic hurricanes. *Tellus,* **50A,** 186–210.
Lunkeit, F., K. Fraedrich, and S. E. Bauer, 1998: Storm tracks in a warmer climate: Sensitivity studies with a simplified global circulation model. *Climate Dyn.,* **14,** 813–826.
Manabe, S., and R. T. Wetherald, 1975: The effects of doubling the CO_2 concentration on the climate of a general circulation model. *J. Atmos. Sci.,* **32,** 3–15.
——, and R. J. Stouffer, 1993: Century-scale effects of increased atmospheric CO_2 on the ocean–atmosphere system. *Nature,* **364,** 215–218.
——, and ——, 1994: Multiple-century response of a coupled ocean–atmosphere model to an increase of atmospheric carbon dioxide. *J. Climate,* **7,** 5–23.
——, and ——, 1996: Low-frequency variability of surface air temperature in a 1000-year integration of a coupled atmosphere–ocean–land surface model. *J. Climate,* **9,** 376–393.
Mason, S. J., and A. M. Joubert, 1997: Simulated changes in extreme rainfall over southern Africa. *Int. J. Climatol.,* **17,** 291–301.
McGuffie, K., A. Henderson-Sellers, N. Holbrook, Z. Kothavala, O. Balachova, and J. Hoekstra, 1999: Assessing simulations of daily temperature and precipitation variability with global climate models for present and enhanced greenhouse climates. *Int. J. Climatol.,* **19,** 1–26.
Mearns, L. O., R. W. Katz, and S. H. Schneider, 1984: Extreme high-temperature events: Changes in their probabilities with changes in mean temperatures. *J. Climate Appl. Meteor.,* **23,** 1601–1613.
——, F. Giorgi, L. McDaniel, and C. Shields, 1995: Analysis of variability and diurnal range of daily temperature in a nested regional climate model: Comparison with observations and doubled CO_2 results. *Climate Dyn.,* **11,** 193–209.
Meehl, G. A., and W. M. Washington, 1996: El Niño-like climate change in a model with increased atmospheric CO_2 concentrations. *Nature,* **382,** 56–60.
——, ——, D. J. Erickson III, B. P. Briegleb, and P. J. Jaumann, 1996: Climate change from increased CO_2 and indirect effects of sulfate aerosols. *Geophys. Res. Lett.,* **23,** 3755–3758.
——, F. Zwiers, J. Evans, T. Knutson, L. Mearns, and P. Whetton, 2000: Trends in extreme weather and climate events: Issues related to modeling extremes in projections of future climate change. *Bull. Amer. Meteor. Soc.,* **81,** 427–436.
Mitchell, J. F. B., T. C. Jones, J. M. Gregory, and S. F. B. Tett, 1995: Climate response to increasing levels of greenhouse gases and sulphate aerosols. *Nature,* **376,** 501–504.
Murphy, J. M., and J. F. B. Mitchell, 1995: Transient response of the Hadley Centre coupled ocean–atmosphere model to increasing carbon dioxide. Part II: Spatial and temporal structure of response. *J. Climate,* **8,** 57–80.
Nicholls, N., G. V. Gruza, J. Jouzel, T. R. Karl, L. Al Ogallo, and D. E. Parker, 1996: Observed climate variability and change. *Climate Change 1995,* J. T. Houghton et al., Eds., Cambridge University Press, 132–192.
Revfeim, K. J. A., and W. D. Hessell, 1984: More realistic distributions for extreme wind gusts. *Quart. J. Roy. Meteor. Soc.,* **110,** 505–514.
Rind, D., R. Goldberg, and R. Ruedy, 1989: Change in climate variability in the 21st century. *Climatic Change,* **14,** 5–37.
Schmittner, A., and T. F. Stocker, 1999: The stability of the ther-

mohaline circulation in global warming experiments. *J. Climate,* **12,** 1117–1133.
Schubert, M., J. Perlwitz, R. Blender, K. Fraedrich, and F. Lunkeit, 1998: North Atlantic cyclones in CO_2-induced warm climate simulations: Frequency, intensity, and tracks. *Climate Dyn.,* **14,** 827–837.
Solman, S. A., and M. N. Nuñez, 1999: Local estimates of global climate change: A statistical downscaling approach. *Int. J. Climatol.,* **19,** 835–861.
Stocker, T. F., and A. Schmittner, 1997: Influence of CO_2 emission rates on the stability of the thermohaline circulation. *Nature,* **388,** 862–865.
Stouffer, R. J., S. Manabe, and K. Ya. Vinnikov, 1994: Model assessment of the role of natural variability in recent global warming. *Nature,* **367,** 634–636.
Taylor, K. E., and J. E. Penner, 1994: Response of the climate system to atmospheric aerosols and greenhouse gases. *Nature,* **369,** 734–737.
Tett, S., 1995: Simulation of El Niño–Southern Oscillation-like variability in a global AOGCM and its response to CO_2 increase. *J. Climate,* **8,** 1473–1502.
Timmermann, A., J. Oberhuber, A. Bacher, M. Esch, M. Latif, and R. Roeckner, 1999: Increased El Niño frequency in a climate model forced by future greenhouse warming. *Nature,* **398,** 694–697.
Ulbrich, U., and M. Christoph, 1999: A shift of the NAO and increasing storm track activity over Europe due to anthropogenic greenhouse gas forcing. *Climate Dyn.,* **15,** 551–559.
Watterson, I. G., 1998: An analysis of the global water cycle of present and doubled CO_2 climates simulated by the CSIRO general circulation model. *J. Geophys. Res.,* **103** (D18), 23 113–23 129.
——, S. P. O'Farrell, and M. R. Dix, 1997: Energy and water transport in climates simulated by a general circulation model that includes dynamic sea ice. *J. Geophys. Res.,* **102** (D10), 11 027–11 037.
Whetton, P. H., A. M. Fowler, M. R. Haylock, and A. B. Pittock, 1993: Implications of climate change due to the enhanced greenhouse effect on floods and droughts in Australia. *Climatic Change,* **25,** 289–317.
Wigley, T. M. L., 1985: Impact of extreme events. *Nature,* **316,** 106–107.
Wood, R. A., A. B. Keen, J. F. B. Mitchell, and J. M. Gregory, 1999: Changing spatial structure of the thermohaline circulation in response to atmospheric CO_2 forcing in a climate model. *Nature,* **399,** 572–575.
Yonetani, T., and H. B. Gordon, 2001: Abrupt changes as indicators of decadal climate variability. *Climate Dyn.,* **17,** 249–250.
Zwiers, F. W., and V. V. Kharin, 1998: Changes in the extremes of the climate simulated by CCC GCM2 under CO_2 doubling. *J. Climate,* **11,** 2200–2222.